ACS APPLIED MATERIALS & INTERFACES

Research Article

www.acsami.org

Self-Assembly of PEI/SiO_2 on Polyethylene Separators for Li-Ion Batteries with Enhanced Rate Capability

Zhuyi Wang,*[,†] Fangling Guo,[†] Cheng Chen,[‡] Liyi Shi,[†] Shuai Yuan,*[,†] Lining Sun,[†] and Jiefang Zhu[§]

[†]Research Centre of Nanoscience and Nanotechnology, Shanghai University, Shanghai 200444, China

[‡]Corning Shanghai Fiber Optics Co., Ltd., Shanghai 200233, China

[§]Ångström Advanced Battery Centre, Uppsala University, 75121 Uppsala, Sweden

Supporting Information

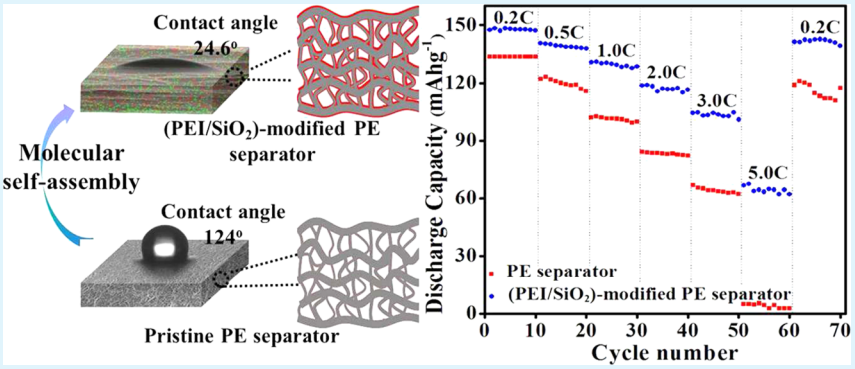

ABSTRACT: A simple and environmentally friendly self-assembly process of oppositely charged polymer PEI and inorganic oxide SiO_2 was demonstrated for the construction of an ultrathin layer on the surface of PE separator. The XPS, FT-IR, SEM, and EDS characterizations give clear evidence of the successful self-assembly of PEI and SiO_2 without significantly increasing the thickness and sacrificing the pristine porous structure of PE separator. This process improves a variety of crucial properties of PE separator such as the electrolyte wetting, the electrolyte uptake, the thermal stability, the ionic conductivity, Li^+ transference number, the electrochemical stability and the compatibility with lithium electrode, endowing lithium-ion battery (Li as anode and $LiCoO_2$ as cathode) with excellent capacity retention at high C-rates and superior cycling performance. At the current density of 5 C, the cell with PE separator almost loses all the capacity. In contrast, the cell with (PEI/SiO_2)-modified PE separator still holds 45.2% of the discharge capacity at 0.2 C. The stabilized SEI formation and high Li^+ transference number of (PEI/SiO_2)-modified PE separator were interpreted to be the substantial reasons leading to the remarkably enhanced battery performance, rendering some new insights into the role of the separator in lithium-ion batteries.

KEYWORDS: *Li-ion battery, rate capability, separator, surface modification, self-assembly*

1. INTRODUCTION

The growing demand for advanced energy storage devices in portable electronics, hybrid electric vehicles and utility grids has stimulated the research and development of lithium-ion batteries (LIBs) with excellent energy density and cycle life.[1−3] As a critical component in rechargeable LIBs, the main function of the separator is to prevent the physical contact between electrodes while enabling Li-ions transport, and avoid the thermal runaway of batteries under overcharge or abnormal heating conditions by thermal shutdown. The properties of the separator determine the electrolyte retention, the cell internal resistance and interface processes involved in cells, and directly affect the safety and electrochemical properties of LIBs.[4,5]

Among various separators developed so far,[6−15] polyolefin separators such as polyethylene (PE) and polypropylene (PP) have been the most predominant ones in commercial LIBs due to their low cost, proper mechanical strength and pore structure, and chemical stability. However, their intrinsically hydrophobic surface character and low surface energy result in poor wettability and retention to polar liquid electrolyte, which could directly impair Li-ions transport through polyolefin separators, and consequently damage the capacity, rate performance and cycle life of LIBs. Moreover, their poor thermal stability often raises serious concern about the safety of LIBs.

To overcome the limitation of conventional polyolefin separators, some efforts focus on grafting some hydrophilic functional groups onto the surface of separators by plasma treatment and electron beam irradiation to improve their electrolyte uptake,[16−18] but the thermal stability of separators is very hard to be improved by this way. The dip-coating of some organic polymers or inorganic oxides with excellent thermal

Received: November 21, 2014
Accepted: January 20, 2015
Published: January 20, 2015

DOI: 10.1021/am508149n
ACS Appl. Mater. Interfaces 2015, 7, 3314−3322

Scheme 1. Schematic Illustrations for (a) Structures of PE Separator before and after Self-Assembly, (b) Experimental Process, and (c) Intermolecular Interactions Occurred in the Process of Self-Assembly

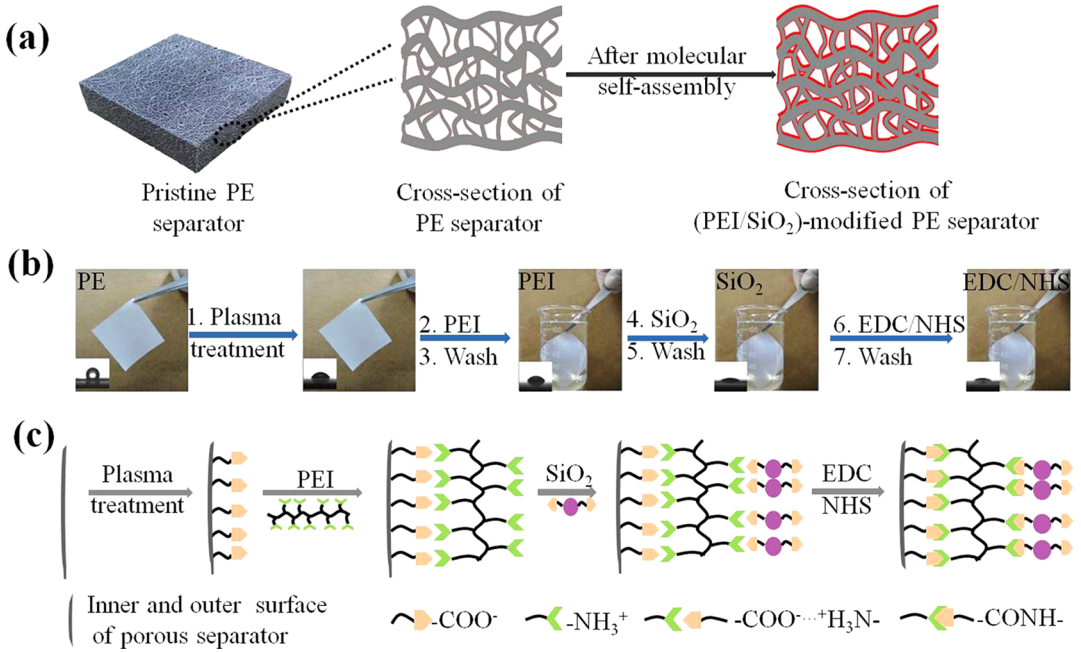

stability or high hydrophilicity on the surface of separators is the focus of attention in recent years for improving the thermal stability and electrolyte uptake of separators.[19,20] However, these processes also generate inevitable negative effects, such as environmental problems due to the use of toxic organic solvents, the significantly increased thickness and pore blocking of separators caused by the use of binders that in turn deteriorate cell performances. For example, Jeong et al.[18] improved the thermal shrinkage and electrolyte uptake of PE separators by a dip-coating process of close-packed SiO_2 nanoparticles interconnected by PVdF-HFP binder, but the modified PE separators show decreased ionic conductance and discharge C-rate capabilities due to their greater thickness (~30 μm) relative to the pristine PE separator (~20 μm), possibly causing long tortuous path for ion transport. Park et al.[21] investigated the effect of the morphological difference between the coating layers on the electrochemical performance of cells. According to their results, the dip-coating of dense PMMA layer on the surface of PE separators improves the electrolyte uptake of separators, but the discharge C-rate capability of cells is deteriorated, owing to the hindrance of ion transport by the nonporous coating layer. Therefore, the thickness and pore structure of separators are directly linked to the battery performance. For high energy and power densities, the separator is required to be thin and highly porous while still remaining mechanically strong, because the thin separator can avoid taking up limited space inside the battery,[5] and the appropriate and uniform pore structure can ensure good ion penetration and uniform current density.[4]

In this paper, a self-assembly process based on the intermolecular forces between oppositely charged polymer and inorganic oxide was demonstrated to provide a powerful tool for the construction of an ultrathin layer on the surface of PE separator. Compared to the aforementioned dip-coating processes, this approach is simpler and its biggest advantage is the ability to exert molecular-level control over the thickness and surface characteristics of the assembled layers. The spontaneous deposition of ultrathin polymer and inorganic oxide layers does not significantly increase the separator thickness, and the original pore structure of PE separator is well-preserved. In addition, the entire self-assembly process was performed in aqueous media and is environmentally friendly. The resulting PE separator exhibits remarkably increased electrolyte uptake and superior electrochemical properties in terms of the ionic conductivity, Li^+ transference number, the electrochemical stability and the compatibility with lithium electrode. By sandwiching this functionalized PE separator between Li anode and $LiCoO_2$ cathode, we developed a half-cell LIB that exhibits excellent capacity retention at high C-rates and superior cycling performance.

2. EXPERIMENTAL SECTION

2.1. Materials. Tetraethoxysilane (TEOS) and lysine were purchased from Sinopharm Chemical Reagent Co., polyethylenimine (PEI, branched, M_W = 25 000 g/mol), 2-(*N*-morpholino)-ethanesulfonic acid (MES), 1-ethyl-3-(3-(dimethylamino)propyl)-carbodiimide hydrochloride (EDC), and *N*-hydroxysuccinimide (NHS) were obtained from Sigma-Aldrich. All these chemicals were used as received without further purification. Li metal foil was obtained from China Energy Lithium Company (Tianjin, China). Liquid electrolyte consisting of 1 M $LiPF_6$ in ethylene carbonate (EC)-diethyl carbonate (DEC)-ethyl methyl carbonate (EMC) (1/1/1 by weight) was purchased from Guotai Huarong Company (Zhangjiagang, China). PE separators were purchased from SK Innovation (14 μm microporous monolayer polyethylene membrane with a porosity of around 50%).

2.2. Synthesis of Carboxyl-Functionalized SiO_2 Colloids. Carboxyl-functionalized SiO_2 colloids were synthesized by a sol−gel process.[22,23] Typically, 11.14 mL TEOS was added into the aqueous solution of lysine (0.148 g L-lysine in 139.2 mL deionized water) in one pot. The resulting mixture was stirred vigorously at 60 °C for 24 h to allow the complete hydrolysis of TEOS to get transparent carboxyl-functionalized SiO_2 colloids.

2.3. Fabrication of (PEI/SiO_2)-Modified PE Separator. Schematic illustration for the fabrication of (PEI/SiO_2)-modified PE separator is shown in Scheme 1. The sequential self-assembly process

DOI: 10.1021/am508149n
ACS Appl. Mater. Interfaces 2015, 7, 3314−3322

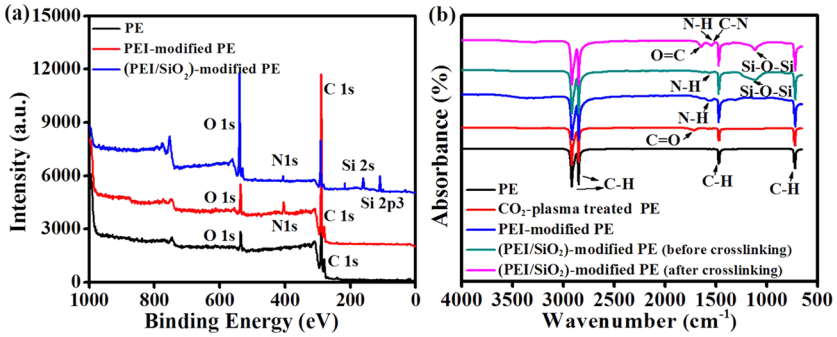

Figure 1. XPS spectra (a) and FT-IR spectra (b) of separators.

of PEI and SiO_2 is driven by the electrostatic force between them. First, PE separators were ultrasonically cleaned with ethanol and deionized water in sequence followed by drying with a stream of nitrogen gas, and then treated by CO_2-plasma (power, 80 W; time, 60 S) to give rise to carboxyl-activated surface. The resulting PE separators were first immersed into the aqueous solution of 1 mg/mL PEI for 20 min to allow the adsorption of PEI and then washed in deionized water to form a primer PEI layer. Subsequently, the PEI-primed PE separators were immersed into 1 mg/mL carboxyl-functionalized SiO_2 colloids for 10 min followed by the same rinse step to obtain (PEI/SiO_2)-modified PE separators. After the self-assembly process, the separators were immersed in a solution consisting of EDC (50 mg/mL) and NHS (50 mg/mL) in MES buffer (0.05 M, pH 5.5, water as the solvent) for 24 h to undergo the interlayer cross-linking through the imidization between carboxyl groups and amino groups.

2.4. Characterization. The morphology and particle size of SiO_2 colloids were observed using transmission electron microscope (TEM, JEOL JEM-200 CX). The zeta potential and size distribution of SiO_2 colloids were measured on a Zetasizer 3000HS (Malvern Instruments Ltd., U.K.). The functional groups on the surface of SiO_2 particles were confirmed by Fourier transformed infrared spectroscopy (FT-IR, Nicolet6700). The chemical composition on the surface of separators after the self-assembly and interlayer cross-linking was analyzed by X-ray photoelectron spectroscopy (XPS, PerkinElmer PHI 5000C ESCA) with Mg Kα radiation and Fourier transformed infrared spectroscopy (FT-IR, Nicolet6700). The surface and cross section porous structure of separators as well as the elemental distribution were examined by scanning electron microscope (SEM) combined with energy dispersive X-ray spectroscopy (EDS) (S-4800). The porosity and pore size distribution of separators were analyzed by mercury intrusion porosimetry (AutoPore IV 9500). The air permeability of separators was evaluated with a Gurley densometer (UEC, 1012A) by measuring the time necessary for air to pass through a determined volume under a given pressure, where a low Gurley value represents high air permeability. The electrolyte wettability of separators was observed by the turbidity change on the surface of separators after dropping the liquid electrolyte and confirmed by a contact angle analyzer (KRUSS, DSA100). The electrolyte uptake of separators was measured by immersing them into the liquid electrolyte separately for 1 h and calculating with the following equation: electrolyte uptake = $100\% \times (W_i - W_o)/W_o$, where W_i represents the weight of the electrolyte-soaked separators, and the extra electrolyte on the surface of separators was wiped with a filter paper before measuring the weight; W_o is the weight of dry separators. The thermal shrinkage of separators was determined by measuring the dimensional change of them after exposure to various temperatures for 0.5 h.

2.5. Electrochemical Measurements. The separators were sufficiently soaked in a liquid electrolyte consisting of 1 M $LiPF_6$ in ethylene carbonate (EC)-diethyl carbonate (DEC)-ethyl methyl carbonate (EMC) (1/1/1 by weight) in an argon-filled glovebox. The ionic conductivity was measured by an AC impedance analysis using an electrochemical workstation (Chenhua, CHI660E) over the frequency range of 1 Hz to 0.1 MHz. The soaked separators were sandwiched between two stainless steel (SS) electrodes and assembled into blocking-type cells. The ionic conductivity was calculated from the following equation: $\sigma = d/R{\cdot}S$, where σ is the ionic conductivity, d is the thickness of separators, R is the bulk resistance, and S is the area of stainless steel electrodes.

The electrochemical stability was measured by the linear sweep voltammetry (LSV) of Li/separator/SS cells between 1 and 6 V (vs Li^+/Li) at a scan rate of 5 mV s^{-1}. The electrolyte-soaked separators were sandwiched between stainless steel as the working electrode and lithium foil as the counter and reference electrodes.

The lithium ion transference number was measured by the combination of chronoamperometry and electrochemical impedance spectra (EIS) of Li/separator/Li cells according to the equation: $t_{Li+} = I_{ss}(\Delta V - I_0R_0)/I_0(\Delta V - I_{ss}R_{ss})$, wherein, I_0 and I_{ss} are the initial and steady-state current obtained by chronoamperometry, respectively; R_0 and R_{ss} are the initial interfacial and steady-state resistance obtained by EIS, respectively; ΔV is the step potential difference (10 mV).

The compatibility of separators with lithium electrode was evaluated by the impedance variation of Li/separator/Li cells over storage at ambient conditions.

Two-electrode coin-type cells were assembled by sandwiching the separators between lithium metal anode and $LiCoO_2$ cathode and then activated by filling the liquid electrolyte. The assembly of cells was carried out in an argon-filled glovebox. The cathode was prepared by coating the *N*-methyl-2-pyrrolidone (NMP)-based slurry consisting of $LiCoO_2$, acetylene black and PVDF in a weight ratio of 8:1:1 on aluminum foil (thickness: 0.014 mm), and the cast foils were then punched into circular pieces (d = 10 mm) and dried at 120 °C for 24 h under vacuum. The mass loading of $LiCoO_2$ was around 3.82 mg/cm^2. The discharge capacity, discharge C-rate capability, and cycling performance of the cells were carried out using the LAND battery cycle system (Wuhan Blue Electric Co., LTD, China). The discharge rates were varied from 0.2 to 5.0 C at a constant charge current density of 0.2 C under a voltage range between 3.0 and 4.2 V. For the measurement of cycling performance, the cells were cycled at a constant charge/discharge current density of 0.5 C/0.5 C. AC impedance analysis of cells was performed by an electrochemical workstation (Princeton Parstat 2273) over the frequency range of 10 mHz to 1 MHz.

3. RESULTS AND DISCUSSION

3.1. Physical Properties of Separators. The structure and morphology of as-prepared SiO_2 colloids were characterized by TEM, Zetasizer and FT-IR (Supporting Information Figure S1). According to the TEM image and the size distribution, the as-prepared SiO_2 colloids show spherical nanoparticles with very small size (around 8 nm) and uniform size distribution. The appearance of characteristic absorption peaks assigned to C═O bond along with Si−O−Si bond confirms the existence of carboxyls on the surface of SiO_2 particles. The Zeta potential of SiO_2 colloids is −27 mV, verifying that SiO_2 colloids possess the sufficient surface negative charge for the electrostatic self-assembly process.

DOI: 10.1021/am508149n
ACS Appl. Mater. Interfaces 2015, 7, 3314−3322

The self-assembly process of PEI and SiO_2 on the surface of PE separator was confirmed by XPS and FT-IR. As shown in Figure 1a, the pristine PE separator just shows the peaks assigned to C 1s and O 1s. The successive appearance of new peaks attributed to N 1s, Si 2s and Si 2p3, and the significant increase in the intensity of O 1s peak indicates that the stepwise self-assembly of PEI and SiO_2 on the surface of PE separator is successful. Figure 1b shows the FT-IR spectra of pristine PE separator and modified PE separators before and after chemical cross-linking. It can be noted that the pristine PE separator just exhibits strong absorption peaks corresponding to the stretching vibration of C−H bond, and the CO_2-plasma treatment of PE separator leads to the appearance of new peak assigned to C═O bond. After PEI was adsorbed onto the surface of CO_2-plasma treated PE separator, a peak at 1565.1 cm^{-1} corresponding to N−H bond appears. Adsorption of SiO_2 on the PEI layer shows the appearance of new peak at 1100 cm^{-1}, ascribed to the stretching vibration of Si−O−Si bond. These results further confirm the successful self-assembly of PEI and SiO_2 on the surface of PE separator. Two additional characteristic absorption peaks assigned to C═O bond and C−N bond due to the formation of O═C-NH bond appear after the chemical cross-linking of (PEI/SiO_2)-modified PE separator, establishing the evidence of interlayer linkages through the imidization between carboxyl groups and amino groups.

Figure 2a−d shows the surface and cross section SEM images of PE separator and (PEI/SiO_2)-modified PE separator. The surface porous structure of PE separator remains almost unchanged after the self-assembly of PEI and SiO_2 and no obvious increase in the thickness of PE separator was observed. The preserved porous structure was further analyzed quantitatively by the measurements of porosity, pore-size distribution and Gurley value. As shown in Table 1 and Supporting Information Figure S2, PE separator shows a slightly increased Gurley value after the self-assembly of PEI and SiO_2, and the porosity and pore-size distribution before and after self-assembly are almost identical, implying that this modification process does not block the original pores of PE separator. This result can be explained by the feature of electrostatic self-assembly technique, which is a process based on the adsorption and desorption balance of charge-containing substances at the solid/liquid interfaces, and can provide the molecular-level control over the film thickness. The thickness of an assembled monolayer is typically several nanometers, such a thickness is negligible relative to the thickness of pristine PE separator, and will not cause the pore blocking issue. To confirm that the self-assembly of PEI and SiO_2 also takes place on the inner surface of the porous separator, energy dispersive X-ray analysis (EDX) was carried out for (PEI/SiO_2)-modified PE separator. As shown in Figure 2e,f, Si and O elements are homogeneously distributed throughout the surface and cross section of (PEI/SiO_2)-modified PE separator, verifying that the self-assembly of PEI and SiO_2 was completed throughout the entire porous surface of PE separator.

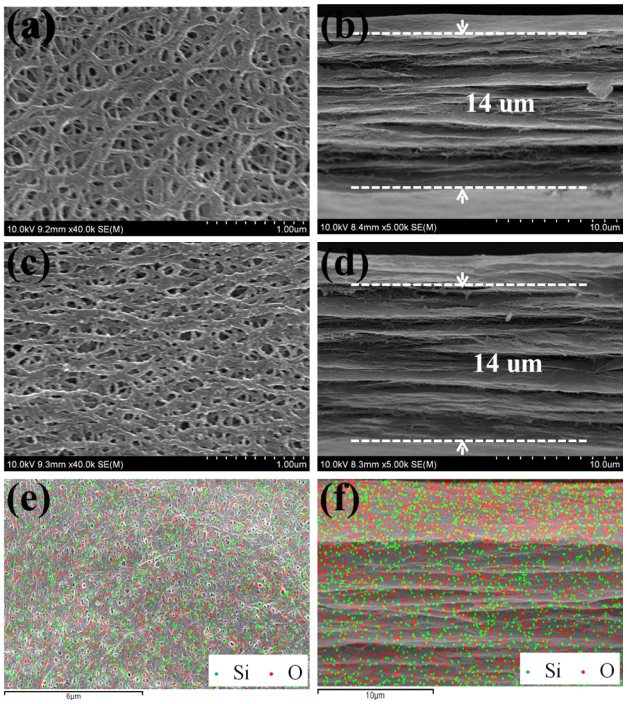

Figure 2. SEM images of the surface (a) and cross section (b) for PE separator, the surface (c) and cross section (d) for (PEI/SiO_2)-modified PE separator, EDX full elemental maps of the surface (e) and cross section (f) for (PEI/SiO_2)-modified PE separator.

The enhanced hydrophilic characteristic of (PEI/SiO_2)-modified PE separator was confirmed by the following results. First, the water contact angle of PE separator decreases from 124° to 24.6° after modification. Second, the liquid electrolyte absorption test (Supporting Information Figure S3) shows that the pristine PE separator is hardly wetted by the liquid electrolyte and forms liquid droplets on the surface owing to its intrinsical hydrophobicity and low surface energy, but (PEI/SiO_2)-modified PE separator is quickly wetted by the liquid electrolyte within 2 s. The enhanced hydrophilic characteristic is attributed to the higher polarity and surface energy after the self-assembly of PEI and SiO_2, which leads to a striking increase in the electrolyte uptake of PE separator from 153% to 398%.

3.2. Electrochemical Properties of Separators. The voltage corresponding to the onset of a steady increase in the observed current density indicates the electrochemical stability limit of the electrolyte-soaked separators. According to the results shown in Figure 3, the electrolyte-soaked PE separator exhibits an anodic stability up to 4.3 V versus Li^+/Li, while the anodic stability for (PEI/SiO_2)-modified PE separator is increased to 4.6 V. This stability enhancement (i.e., better compatibility with the cathode of Li-ion battery) may be attributed to the excellent electrolyte affinity of (PEI/SiO_2)-modified PE separator and the stabilization of electrolyte anions by Lewis acid centers. The free solvent molecules in the liquid electrolyte tend to be decomposed on the cathode of lithium ion battery,[24,25] the excellent electrolyte uptake of (PEI/SiO_2)-modified PE separator can reduce the decomposition of solvent molecules on the cathode of lithium ion battery. Moreover, the Si−O units on the surface of (PEI/SiO_2)-modified PE separator can act as Lewis acid centers to trap lithium salt anions,[26,27] thus delaying the irreversible oxidative decomposition of electrolyte anions.

Supporting Information Figure S4 shows the Nyquist curves of SS/separator/SS cells assembled with the pristine PE separator and modified PE separator. The high-frequency intercept of the Nyquist curves on the Z' axis represents the bulk resistance R. The ionic conductivity of the liquid electrolyte-soaked PE separator and (PEI/SiO_2)-modified PE separator was calculated from the bulk resistance to be 0.36 and 0.49 mS cm^{-1} (Table 1) at 25 °C, respectively. The ionic conductivity of microporous PE separator greatly depends on

DOI: 10.1021/am508149n
ACS Appl. Mater. Interfaces 2015, 7, 3314−3322

Table 1. Properties of PE Separator and (PEI/SiO_2)-Modified PE Separator

sample	porosity (%)	Gurley value (s 100 cc^{-1})	contact angle	electrolyte uptake (%)	ionic conductivity (mS cm^{-1})	lithium transference number
PE separator	47.63	226	124°	153	0.36	0.36
(PEI/SiO_2)-modified PE separator	47.63	280	24.6°	398	0.49	0.66

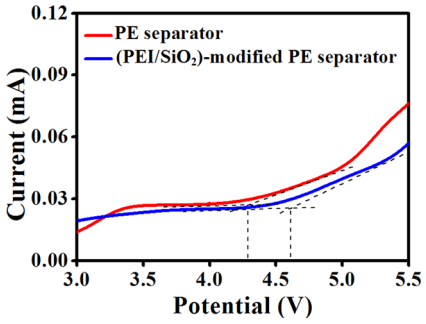

Figure 3. Linear sweep voltammetry (LSV) curves of Li/electrolyte-soaked separator/SS cells assembled with PE separator and (PEI/SiO_2)-modified PE separator.

the pore structure and electrolyte uptake. As shown in SEM results, the electrostatic self-assembly of PEI and SiO_2 on the surface of PE separator maximally preserves its pristine porous structure and thickness, and significantly increases its electrolyte uptake, which synergistically contributes to the enhanced ionic conductivity of PE separator.

The Li^+ transference number (t_{Li+}) estimated by the combination of chronoamperometry and EIS of Li/separator/Li cells (Figure 4) is shown in Table 1. The calculated t_{Li+}

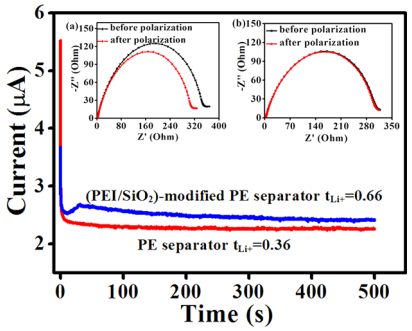

Figure 4. Chronoamperometry of Li/electrolyte-soaked separator/Li cells at 25 °C. Inset: EIS for the same cells before and after polarization assembled with (a) PE separator and (b) (PEI/SiO_2)-modified PE separator.

values for the electrolyte-soaked PE separator and (PEI/SiO_2)-modified PE separator are 0.36 and 0.66, respectively. The higher t_{Li+} of (PEI/SiO_2)-modified PE separator suggests a higher Li^+ transport ability, and it benefits from the excellent electrolyte affinity of (PEI/SiO_2)-modified PE separator and the aforementioned trapping effect of electrolyte anions by Si–O units on the separator surface as Lewis acid centers, which allows a higher fraction of Li^+ to be available for the conduction.

The compatibility of liquid electrolyte-soaked separators with lithium electrode was investigated by evaluating the impedance variation of Li/liquid electrolyte-soaked separator/Li cells over storage time as shown in Figure 5. A semicircle was observed from the impedance spectra of cells with both separators that represents the Li/electrolyte interfacial resistance (R_{int}), which was related to the charge transport across the passivation layer (solid electrolyte film) and the charge transfer reaction, $Li^+ + e^- = Li$. The initial R_{int} for PE separator and (PEI/SiO_2)-modified PE separator is 292 and 248 Ω, respectively, and the increase in R_{int} with storage time reflects the growth of the passivation layer due to the reaction between electrolyte components and the lithium electrode. The R_{int} for electrolyte-soaked (PEI/SiO_2)-modified PE separator gets stabilized (3825 Ω) after 6 days of storage, indicating the tendency to form a stable solid electrolyte film as time proceeds, while the R_{int} for electrolyte-soaked PE separator continuously and rapidly increases with storage time and reaches the maximum of 16 916 Ω after 7 days. This result demonstrates that (PEI/SiO_2)-modified PE separator has much better interfacial compatibility with the lithium electrode on continued storage. The compatibility improvement benefits from the excellent electrolyte uptake of (PEI/SiO_2)-modified PE separator, which can effectively decrease the interaction between electrolyte components and the lithium electrode due to a smaller amount of liquid electrolyte in contact with the lithium electrode, and gradually stabilizes the interface.

3.3. Battery Performance. Figure 6a,b depicts the discharge profiles of cells assembled with the pristine PE separator and (PEI/SiO_2)-modified PE separator, and Figure 6c summarizes discharge C-rate capabilities of both separators. The cells were charged under a voltage range between 3.0 and 4.2 V at a constant charge current density of 0.2 C and discharged at various current densities ranging from 0.2 to 5.0 C. For both of the separators, the voltage and discharge capacity of cells gradually decrease with the increase of discharge current density. It is noteworthy that (PEI/SiO_2)-modified PE separator presents larger discharge capacities over various discharge current densities from 0.2 to 5 C, reflecting higher cathode utilization and discharge C-rate capabilities, and the difference in the discharge capacities between two separators becomes larger at higher current densities where the influence of ionic transport on the ohmic polarization (i.e., IR drop) is more significant.[28,29] At the current density of 5 C, PE separator almost loses all the capacity. In contrast, (PEI/SiO_2)-modified PE separator still holds 45.2% of the discharge capacity at 0.2 C. The affecting factors of separators on the C-rate capacity of cells include the ion conductivity and Li-ions transfer through the separator/electrode interface. As shown in Supporting Information Figure S4 and Figures 4 and 5, the higher ion conductivity and Li-ions transference number of (PEI/SiO_2)-modified PE separator can allow faster mobility of Li-ions inside the separator and reduce the polarization caused by the counteranions. Furthermore, the smaller interfacial resistance of the modified PE separator with the lithium electrode means better contact between the separator surface and the electrode, facilitating Li-ions diffusion through the separator/electrode interface. These advantageous characteristics contribute to the higher discharge capacity of cells employing (PEI/SiO_2)-modified PE separator. The cycling performance of cells assembled with these two separators was

DOI: 10.1021/am508149n
ACS Appl. Mater. Interfaces 2015, 7, 3314–3322

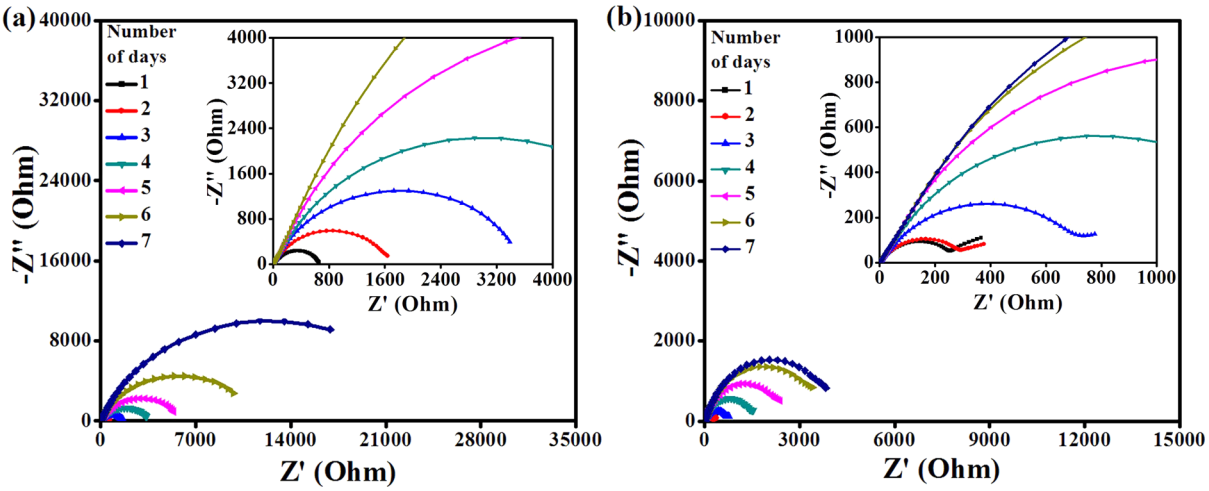

Figure 5. Nyquist plots of Li/electrolyte-soaked separator/Li cells at 25 °C assembled with (a) PE separator, (b) (PEI/SiO_2)-modified PE separator. Inset: the magnified view.

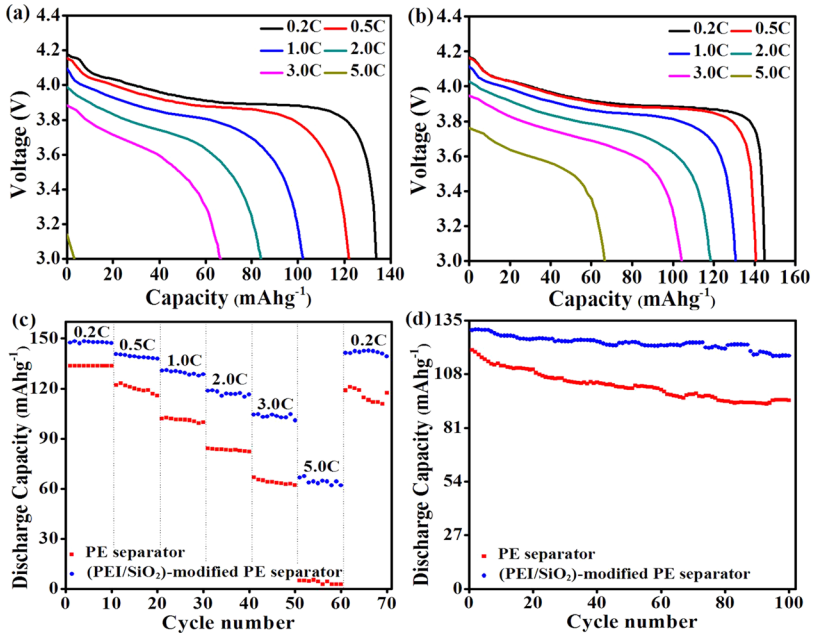

Figure 6. Discharge profiles of cells assembled with (a) PE separator; (b) (PEI/SiO_2)-modified PE separator, (c) comparison of discharge C-rate capabilities between cells assembled with different separators, (d) cycle performance of cells assembled with different separators.

also investigated under a voltage range of 3.0−4.2 V at a constant charge current density of 0.5 C (Figure 6 d). (PEI/SiO_2)-modified PE separator exhibits higher capacity retention during cycling as compared to PE separator, and the discharge capacity retention is found to be 79% for PE separator and 90.1% for (PEI/SiO_2)-modified PE separator after the 100th cycle. The columbic efficiency (Supporting Information Figure S5) of the cell assembled with (PEI/SiO_2)-modified PE separator at 0.5 C was maintained around 98.8% throughout the cycling process, reflecting high charge-transfer reversibility at electrode/separator interface.

To give more insights into the superior discharge C-rate capability and cycling performance of (PEI/SiO_2)-modified PE separator relative to the pristine PE separator, the AC impedance spectra of cells assembled with these two separators after different cycles were analyzed. According to the results shown in Figure 7, both Nyquist plots are clearly composed of two semicircles in the high-middle frequency and an inclined

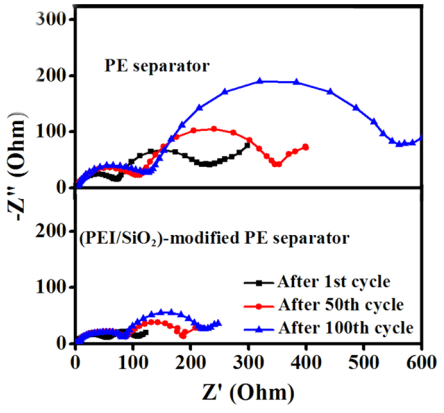

Figure 7. Variation in AC impedance spectra (1st cycle-50th cycle-100th cycle) of cells assembled with PE separator and (PEI/SiO_2)-modified PE separator.

DOI: 10.1021/am508149n
ACS Appl. Mater. Interfaces 2015, 7, 3314−3322

Table 2. Resistance Data of Cells Assembled with PE Separator and (PEI/SiO_2)-Modified PE Separator

cell		R_b (Ohm)	R_{SEI} (Ohm)	R_{ct} (Ohm)	R (Ohm)[a]
Li/PE separator/$LiCoO_2$	After 1st cycle	1.70	72	165	238.7
	After 50th cycle	1.92	112	238	351.9
	After 100th cycle	2.26	125	435	562.3
Li/(PEI/SiO_2)-modified PE separator/$LiCoO_2$	After 1st cycle	1.63	55	55	111.6
	After 50th cycle	1.77	86	98	185.8
	After 100th cycle	1.78	85	135	221.8

[a]R represents the total internal resistance of cells (R_b + R_{SEI} + R_{ct}).

line in the low frequency region. The high-frequency semicircles (left) represent the resistance through the SEI layers (R_{SEI}), the middle-frequency semicircles (right) represent the charge-transfer resistance (R_{ct}) associated with the migration of Li ions at the electrode−electrolyte interfaces, and the straight lines represent the Warburg impedance (W_0). The intercept of Nyquist curves at Z' axis represents the combination resistance R_b related to the ionic resistance of the electrolyte, the intrinsic resistance of the active materials and the contact resistance at the active material/current collector interface.[30−32] The summation of R_b, R_{SEI}, and R_{ct} gives the overall internal resistance of cells, and the low capacity and strong decay at high C-rates is an indication of increased cell internal resistance. According to the resistance data shown in Table 2, the R_b is negligible relative to the total resistance, so the R_{SEI} and R_{ct} are the dominant factors affecting the battery rate capability. The cell assembled with PE separator shows much higher R_{SEI} and R_{ct} than that assembled with (PEI/SiO_2)-modified PE separator, and the R_{SEI} and R_{ct} significantly increase as cell cycles to the 100th (from 72 to 125 Ω for R_{SEI}, 165 to 435 Ω for R_{ct}). On the contrary, the R_{SEI} and R_{ct} for the cell with (PEI/SiO_2)-modified PE separator show a rise at a much lower increment rate. The R_{SEI} for the cell with (PEI/SiO_2)-modified PE separator gets stabilized after 50th cycle, which means a more stable and suppressed SEI-layer formation, facilitating Li^+ transport through the interfacial layer. More evidence of good SEI stability can be found by the morphological analysis of the cycled lithium anode. Figure 8 shows SEM images of lithium metal electrodes disassembled from cells employing both separators after 100th cycle.

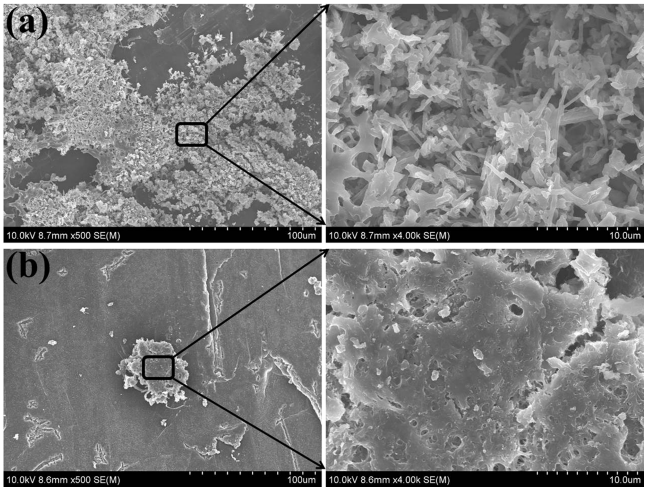

Figure 8. SEM images of lithium−metal electrodes disassembled from cells after 100th cycle employing (a) PE separator and (b) (PEI/SiO_2)-modified PE separator.

According to the results, the lithium electrode surface of the cell with the modified separator still remains smooth without dendrites after 100 cycles, although there are some Li bumps. In contrast, the lithium electrode surface of the cell with the pristine separator shows the formation of dendrites with rod-like morphologies. This morphological difference reveals that the dendrite growth during cycling can be effectively suppressed by the modification of PE separator. The smaller R_{ct} of the cell with (PEI/SiO_2)-modified PE separator indicates faster charge transfer at the electrolyte/electrode interface, which is partially attributed to the much larger t_{Li+} of (PEI/SiO_2)-modified PE separator. The barrier potential caused by the migration and accumulation of counteranions in the vicinity of the electrode−electrolyte interface is a key factor hindering the motion of Li^+, and this phenomenon is more visible at high C-rates and leads to high internal resistance that ultimately limits the charging rates and energy density of batteries. High t_{Li+} can decrease the electrode polarization caused by anions accumulation and suppress the anion concentration gradient to facilitate Li^+ transport, and is beneficial for the battery to work under high current density.[33−37]

Therefore, it is substantially the stabilized SEI formation and high t_{Li+} that suppress the electrode polarization at high discharge rates and accordingly lower the cell resistance, rendering the cell with (PEI/SiO_2)-modified PE separator higher capacity retention at high C-rates. As for the cycle performance, the growth of dendrites at the electrolyte/electrode interface during cycling is the origin of rapid interface deterioration and capacity fading.[38] The suppressed dendrites growth mainly accounts for the better cycle performance of the cell with (PEI/SiO_2)-modified PE separator.

In addition to the improved battery performance, it has also been found that the self-assembly of PEI and SiO_2 on the surface of PE separator endows PE separator with an improved thermal stability after the thermal treatment at different temperatures for 0.5 h (Supporting Information Figure S6). The enhanced thermal stability is due to the good thermal stability of PEI and SiO_2 layers on the PE matrix, which plays a positive role in holding the overall skeleton of PE separator and therefore provides the enhanced resistance against thermal shrinkage.

4. CONCLUSIONS

A simple and environmentally friendly molecular self-assembly process of oppositely charged polymer PEI and inorganic oxide SiO_2 was demonstrated to improve a variety of crucial properties of PE separator such as the electrolyte wetting, the electrolyte uptake, the thermal stability, the ionic conductivity, Li^+ transference number, the electrochemical stability and the compatibility with lithium electrode. When the structure and properties of PE separator were correlated with the battery performance, the stabilized SEI formation and high Li^+

DOI: 10.1021/am508149n
ACS Appl. Mater. Interfaces 2015, 7, 3314−3322

transference number ensured by the well-preserved porous structure and remarkably enhanced electrolyte uptake were found to substantially suppress the electrode polarization and lower the cell resistance and, therefore, render the battery more favorable capacity retention at high C-rates and superior cycling performance. This study not only provides a better understanding of the role of the separator in Li-ion batteries but also demonstrates a powerful and versatile approach applicable to other separators or substrates with similar surface property issues.

■ ASSOCIATED CONTENT

Supporting Information

TEM, FT-IR spectrum, size distribution and zeta potential of SiO_2 colloids; pore-size distribution; liquid electrolyte wettability; Nyquist plots of SS/separator/SS cells; thermal shrinkage for PE separator and (PEI/SiO_2)-modified PE separator; Coulomb efficiency of Li/(PEI/SiO_2)-modified PE separator/$LiCoO_2$ cell. This material is available free of charge via the Internet at http://pubs.acs.org.

■ AUTHOR INFORMATION

Corresponding Authors

*E-mail: bamboo2009@shu.edu.cn. Tel: +86 21 66136082.
*E-mail: s.yuan@shu.edu.cn. Tel: +86 21 66136082.

Notes

The authors declare no competing financial interest.

■ ACKNOWLEDGMENTS

The authors acknowledge Professor Kristina Edström and Torbjörn Gustafsson of Uppsala University for the helpful discussion, and the support of Natural Science Foundation of Shanghai (13ZR1454400), International cooperation fund of Shanghai Science and Technology Committee (14520722200), Shanghai Municipal Science and Technology Commission (13DZ2292100), National Natural Science Foundation of China (21102088).

■ REFERENCES

(1) Armand, M.; Tarascon, J.-M. Building Better Batteries. *Nature* **2008**, *451*, 652−657.
(2) Thackeray, M. M.; Wolverton, C.; Isaacs, E. D. Electrical Energy Storage for Transportation-Approaching the Limits of, and Going Beyond, Lithium-Ion Batteries. *Energy Environ. Sci.* **2012**, *5*, 7854−7863.
(3) Scrosati, B.; Hassoun, J.; Sun, Y.-K. Lithium-Ion Batteries. A Look into the Future. *Energy Environ. Sci.* **2011**, *4*, 3287−3295.
(4) Arora, P.; Zhang, Z. M. Battery Separators. *Chem. Rev.* **2004**, *104*, 4419−4462.
(5) Zhang, S. S. A Review on the Separators of Liquid Electrolyte Li-Ion Batteries. *J. Power Sources* **2007**, *164*, 351−364.
(6) Zhu, Y. S.; Wang, F. X.; Liu, L. L.; Xiao, S. Y.; Chang, Z.; Wu, Y. P. Composite of a Nonwoven Fabric with Poly(vinylidene fluoride) as a Gel Membrane of High Safety for Lithium Ion Battery. *Energy Environ. Sci.* **2013**, *6*, 618−624.
(7) Jiang, W.; Liu, Z. H.; Kong, Q. S.; Yao, J. H.; Zhang, C. J.; Han, P. X.; Cui, G. L. A High Temperature Operating Nanofibrous Polyimide Separator in Li-Ion Battery. *Solid State Ionics* **2013**, *232*, 44−48.
(8) Zhang, J. J.; Liu, Z. H.; Kong, Q. S.; Zhang, C. J.; Pang, S. P.; Yue, L. P.; Wang, X. J.; Yao, J. H.; Cui, G. L. Renewable and Superior Thermal-Resistant Cellulose-Based Composite Nonwoven as Lithium-Ion Battery Separator. *ACS Appl. Mater. Interfaces* **2013**, *5*, 128−134.
(9) He, M.; Zhang, X.; Jiang, K.; Wang, J.; Wang, Y. Pure Inorganic Separator for Lithium Ion Batteries. *ACS Appl. Mater. Interfaces* **2015**, 7 (1), 738−742 DOI: 10.1021/am507145h.
(10) Woo, J.-J.; Zhang, Z.; DietzRago, N. L.; Lu, W.; Amine, K. A High Performance Separator with Improved Thermal Stability for Li-Ion Batteries. *J. Mater. Chem. A* **2013**, *1*, 8538−8540.
(11) Xu, Q.; Kong, Q.; Liu, Z.; Wang, X.; Liu, R.; Zhang, J.; Yue, L.; Duan, Y.; Cui, G. Cellulose/Polysulfonamide Composite Membrane as a High Performance Lithium-Ion Battery Separator. *ACS Sustainable Chem. Eng.* **2014**, *2*, 194−199.
(12) Zhang, J.; Yue, L.; Kong, Q.; Liu, Z.; Zhou, X.; Zhang, C.; Xu, Q.; Zhang, B.; Ding, G.; Qin, B.; Duan, Y.; Wang, Q.; Yao, J.; Cui, G.; Chen, L. Sustainable, Heat-Resistant and Flame-Retardant Cellulose-Based Composite Separator for High-Performance Lithium Ion Battery. *Sci. Rep.* **2014**, *4*, 3935−3942.
(13) Yanilmaz, M.; Lu, Y.; Li, Y.; Zhang, X. SiO_2/Polyacrylonitrile Membranes via Centrifugal Spinning as a Separator for Li-Ion Batteries. *J. Power Sources* **2015**, *273*, 1114−1119.
(14) Costa, C. M.; Silva, M. M.; Lanceros-Méndez, S. Battery Separators Based on Vinylidene Fluoride (VDF) Polymers and Copolymers for Lithium Ion Battery Applications. *RSC Adv.* **2013**, *3*, 11404−11417.
(15) Zhai, Y.; Wang, N.; Mao, X.; Si, Y.; Yu, J.; Al-Deyab, S. S.; El-Newehy, M.; Ding, B. Sandwich-Structured PVdF/PMIA/PVdF Nanofibrous Separators with Robust Mechanical Strength and Thermal Stability for Lithium Ion Batteries. *J. Mater. Chem. A* **2014**, *2*, 14511−14518.
(16) Lee, J. Y.; Lee, Y. M.; Bhattacharya, B.; Nho, Y.-C.; Park, J.-K. Separator Grafted with Siloxane by Electron Beam Irradiation for Lithium Secondary Batteries. *Electrochim. Acta* **2009**, *54*, 4312−4315.
(17) Kim, J. Y.; Lee, Y.; Lim, D. Y. Plasma-Modified Polyethylene Membrane as a Separator for Lithium-Ion Polymer Battery. *Electrochim. Acta* **2009**, *54*, 3714−3719.
(18) Jeong, H.-S.; Lee, S.-Y. Closely Packed SiO_2 Nanoparticles/Poly(vinylidene fluoride-hexafluoropropylene) Layers-Coated Polyethylene Separators for Lithium-Ion Batteries. *J. Power Sources* **2011**, *196*, 6716−6722.
(19) Kim, K. J.; Kwon, H. K.; Park, M. S.; Yim, T.; Yu, J. S.; Kim, Y. J. Ceramic Composite Separators Coated with Moisturized ZrO_2 Nanoparticles for Improving the Electrochemical Performance and Thermal Stability of Lithium Ion Batteries. *Phys. Chem. Chem. Phys.* **2014**, *16*, 9337−9343.
(20) Fang, L.-F.; Shi, J.-L.; Jiang, J.-H.; Li, H.; Zhu, B.-K.; Zhu, L.-P. Improving the Wettability and Thermal Resistance of Polypropylene Separators with a Thin Inorganic-Organic Hybrid Layer Stabilized by Polydopamine for Lithium Ion Batteries. *RSC Adv.* **2014**, *4*, 22501−22508.
(21) Park, J.-H.; Park, W.; Kim, J. H.; Ryoo, D.; Kim, H. S.; Jeong, Y. U.; Kim, D.-W.; Lee, S.-Y. Close-Packed Poly(methyl methacrylate) Nanoparticle Arrays-Coated Polyethylene Separators for High-Power Lithium-Ion Polymer Batteries. *J. Power Sources* **2011**, *196*, 7035−7038.
(22) Davis, T. M.; Snyder, M. A.; Krohn, J. E.; Tsapatsis, M. Nanoparticles in Lysine-Silica Sols. *Chem. Mater.* **2006**, *18*, 5814−5816.
(23) Yokoi, T.; Wakabayashi, J.; Otsuka, Y.; Fan, W.; Iwama, M.; Watanabe, R.; Aramaki, K.; Shimojima, A.; Tatsumi, T.; Okubo, T. Mechanism of Formation of Uniform-Sized Silica Nanospheres Catalyzed by Basic Amino Acids. *Chem. Mater.* **2009**, *21*, 3719−3729.
(24) Xing, L. D.; Li, W. S.; Wang, C. Y.; Gu, F. L.; Xu, M. Q.; Tan, C. L.; Yi, J. Theoretical Investigations on Oxidative Stability of Solvents and Oxidative Decomposition Mechanism of Ethylene Carbonate for Lithium Ion Battery Use. *J. Phys. Chem. B* **2009**, *113*, 16596−16602.
(25) Xing, L. D.; Wang, C. Y.; Li, W. S.; Xu, M. Q.; Meng, X. L.; Zhao, S. F. Theoretical Insight into Oxidative Decomposition of Propylene Carbonate in the Lithium. *J. Phys. Chem. B* **2009**, *113*, 5181−5187.
(26) Qiu, W. L.; Ma, X. H.; Yang, Q. H.; Fu, Y. B.; Zong, X. F. Novel Preparation of Nanocomposite Polymer Electrolyte and its Application to Lithium Polymer Batteries. *J. Power Sources* **2004**, *138*, 245−252.

(27) Lee, J. Y.; Ko, D.-H.; Lee, Y. M.; Seol, W.-H.; Park, J.-K. New Crosslinking Agent as a Lewis Acid for Solid Polymer Electrolytes. *J. Power Sources* **2007**, *174*, 603−606.
(28) Jeong, H.-S.; Kim, D.-W.; Jeong, Y. U.; Lee, S.-Y. Effect of Phase Inversion on Microporous Structure Development of Al_2O_3/Poly-(vinylidene fluoride-hexafluoropropylene)-Based Ceramic Composite Separators for Lithium-Ion Batteries. *J. Power Sources* **2010**, *195*, 6116−6121.
(29) Choi, E.-S.; Lee, S.-Y. Particle Size-Dependent, Tunable Porous Structure of a SiO_2/Poly(vinylidene fluoride-hexafluoropropylene)-Coated Poly(ethylene terephthalate) Nonwoven Composite Separator for a Lithium-Ion Battery. *J. Mater. Chem.* **2011**, *21*, 14747−14754.
(30) Wang, Y.-X.; Huang, L.; Sun, L.-C.; Xie, S.-Y.; Xu, G.-L.; Chen, S.-R.; Xu, Y.-F.; Li, J.-T.; Chou, S.-L.; Dou, S.-X.; Sun, S.-G. Facile Synthesis of a Interleaved Expanded Graphite-Embedded Sulphur Nanocomposite as Cathode of Li-S Batteries with Excellent Lithium Storage Performance. *J. Mater. Chem.* **2012**, *22*, 4744−4750.
(31) Kim, J.; Lee, D.-J.; Jung, H.-G.; Sun, Y.-K.; Hassoun, J.; Scrosati, B. An Advanced Lithium-Sulfur Battery. *Adv. Funct. Mater.* **2013**, *23*, 1076−1080.
(32) Zhang, L. L.; Zhao, S.; Tian, X. N.; Zhao, X. S. Layered Graphene Oxide Nanostructures with Sandwiched Conducting Polymers as Supercapacitor Electrodes. *Langmuir* **2010**, *26*, 17624−17628.
(33) Wang, S. H.; Hou, S. S.; Kuo, P. L.; Teng, H. Poly(ethylene oxide)-co-Poly(propylene oxide)-Based Gel Electrolyte with High Ionic Conductivity and Mechanical Integrity for Lithium-Ion Batteries. *ACS Appl. Mater. Interfaces* **2013**, *5*, 8477−8485.
(34) Schaefer, J. L.; Yanga, D. A.; Archer, L. A. High Lithium Transference Number Electrolytes via Creation of 3-Dimensional, Charged, Nanoporous Networks from Dense Functionalized Nanoparticle Composites. *Chem. Mater.* **2013**, *25*, 834−839.
(35) Heitner, K. L. The Search for the Better Polymer Electrolyte. *J. Power Sources* **2000**, *89*, 128−131.
(36) Thomas, K. E.; Sloop, S. E.; Kerr, J. B.; Newman, J. Comparison of Lithium-Polymer Cell Performance with Unity and Nonunity Transference Numbers. *J. Power Sources* **2000**, *89*, 132−138.
(37) Tan, S.; Walus, S.; Hilborn, J.; Gustafsson, T.; Brandell, D. Poly(ether amine) and Cross-Linked Poly(propylene oxide) Diacrylate Thin-Film Polymer Electrolyte for 3D-Microbatteries. *Electrochem. Commun.* **2010**, *12*, 1498−1500.
(38) Xu, W.; Wang, J.; Ding, F.; Chen, X.; Nasybulin, E.; Zhang, Y.; Zhang, J.-G. Lithium Metal Anodes for Rechargeable Batteries. *Energy Environ. Sci.* **2014**, *7*, 513−537.

DOI: 10.1021/am508149n
ACS Appl. Mater. Interfaces 2015, 7, 3314−3322